Optics Letters

Accelerated Richardson–Lucy deconvolution by unmatched projection pairs for 3D fluorescence microscopy

Heheng Du,[1,2,3] Ning Zhou,[1,2,3] Hanci Tang,[1,2,3] Zihao Zhou,[1,2,3] Mingyang Xu,[1,2,3] Qian Chen,[1,2,3,4] Runnan Zhang,[1,2,3,4,5] and Chao Zuo[1,2,3,4,*]

[1]Smart Computational Imaging Laboratory (SCILab), School of Electronic and Optical Engineering, Nanjing University of Science and Technology, Nanjing, Jiangsu Province 210094, China
[2]Smart Computational Imaging Research Institute (SCIRI) of Nanjing University of Science and Technology, Nanjing, Jiangsu Province 210019, China
[3]Jiangsu Key Laboratory of Visual Sensing & Intelligent Perception, Nanjing, Jiangsu Province 210094, China
[4]State Key Laboratory of Extreme Environment Optoelectronic Dynamic Measurement Technology and Instrument, Taiyuan, Shanxi Province 030051, China
[5]runnanzhang@njust.edu.cn
*zuochao@njust.edu.cn

Received 15 December 2025; revised 29 January 2026; accepted 5 February 2026; posted 5 February 2026; published 20 February 2026

The Richardson–Lucy deconvolution (RLD) algorithm is widely used in fluorescence microscopy to enhance image sharpness, yet its high computational complexity limits scalability for large three-dimensional (3D) datasets and impedes real-time volumetric visualization. Here, we introduce an accelerated RLD approach using a Wiener–Butterworth unmatched backprojector, termed WB-ARL, which flattens the spectral product between the forward and backprojectors while effectively suppressing high-frequency noise beyond the diffraction limit. WB-ARL reduces the number of iterations required by more than 10-fold compared with conventional RLD while maintaining high-fidelity reconstruction. CUDA acceleration further increases the speed of both methods by 40-fold while maintaining our method's iterative advantage for up to 400× increase over non-CUDA accelerated matched backprojectors. We further analyze its robustness to noise and optical aberrations and validate its performance through 3D reconstructions of both wide-field mouse kidney tissue and confocal cell phantoms. Our results demonstrate that WB-ARL enables high-resolution, high-fidelity 3D imaging with significantly reduced computational cost, offering a scalable solution for high-throughput fluorescence microscopy.

https://doi.org/10.1364/OL.587803

Real-time, high-resolution 3D fluorescence imaging is essential for studying complex biological structures and dynamics [1–3]. In fluorescence microscopy, the recorded volume can be modeled as a convolution between the underlying object and the system point spread function (PSF), corrupted by noise. Deconvolution is therefore routinely applied to restore contrast and approach diffraction-limited resolution. Among available methods, Richardson–Lucy deconvolution (RLD), which admits a maximum-likelihood formulation under Poisson noise, is widely used in 3D fluorescence imaging [4–6].

Despite its effectiveness, conventional 3D RLD is often prohibitively slow for large volumes, as each iteration requires repeated forward and backward projections and many iterations are typically needed to reach a satisfactory solution [7,8]. Hardware acceleration, such as GPU parallelism, can reduce the per-iteration cost but does not address the fundamental issue that the iteration count remains high [9]. Algorithmic accelerations such as extrapolation or momentum can reduce iterations but may become unstable and often require additional safeguards [10–12]. A key reason for slow convergence in standard RLD is that the forward projector and its matched backprojector yield a spectral product that rapidly decays at high spatial frequencies due to the weak high-frequency response of the optical transfer function (OTF), resulting in poor eigenvalue clustering and thus slow iterative progress [13].

Here we present a Wiener–Butterworth accelerated RLD (WB-ARL) algorithm based on an unmatched backprojector design. Our central idea is to construct a backprojector whose frequency response flattens the spectral product with the system OTF within the passband while suppressing excessive gain beyond the diffraction limit, thereby improving eigenvalue clustering and accelerating convergence [14–16]. WB-ARL reduces the required iteration number by more than an order of magnitude compared with conventional RLD while maintaining reconstruction fidelity. By combining this algorithm with CUDA-based parallel acceleration, the end-to-end processing speed reaches up to ~400× compared with CPU-based conventional implementations for volumes with tens of millions of voxels. We further analyze robustness to noise and optical aber-

rations, and validate WB-ARL through 3D reconstructions of both wide-field mouse kidney tissue and confocal cell phantoms.

In iterative reconstruction, the forward projector F models the imaging physics, whereas the backprojector B can be relaxed without compromising convergence, leading to unmatched projector/backprojector schemes that significantly accelerate convergence and reduce computational burden [14,17,18]. A general linear iterative update can be written as:

$$X^{(k+1)} = X^{(k)} + SB^T(P - FX^{(k)}), \tag{1}$$

where S is a diagonal step-size matrix. Defining $M = I - SB^TF$, convergence is guaranteed when the spectral radius $\rho(M) < 1$, and the convergence rate is governed by the eigenvalue distribution of B^TF. Faster convergence is achieved when these eigenvalues cluster tightly, motivating the use of carefully designed unmatched backprojectors (See S1 of Supplement 1 for details).

A well-known example of an unmatched projector/backprojector scheme is the maximum-likelihood expectation-maximization (ML-EM) algorithm and the RLD algorithm is a special case of it. In wide-field fluorescence microscopy, the imaging process can be modeled as a linear space-invariant system $i = o \otimes f + n$, where f is the point spread function. Conventional RLD employs matched projector/backprojector pairs, for which the eigenvalue spectrum of B^TF decays rapidly at high spatial frequencies due to the OTF, resulting in slow convergence.

To accelerate RLD, we design an unmatched backprojector such that the spectrum of B^TF is flattened within the passband (see S2 of Supplement 1 for details). Since convolution operators are diagonalizable in the Fourier domain, this problem reduces to designing a frequency-domain backprojector $B(k)$ that approximates the inverse of the OTF while suppressing excessive high-frequency amplification. We formulate this as a regularized inverse problem:

$$\min_{B(k)} \|B(k)F(k) - 1\|_2^2 + \lambda \|W(k)B(k)\|_2^2, \tag{2}$$

where $W(k)$ is a Butterworth-type weighting function that penalizes gain beyond the diffraction limit. This yields the closed-form solution:

$$B^*(k) = \frac{\overline{F(k)}}{|F(k)|^2 + \lambda W^2(k)}. \tag{3}$$

This design explicitly improves the eigenvalue clustering of the composite operator B^TF, which directly governs the convergence rate of the iterative update in Eq. (1). The resulting WB backprojector generalizes the classical Wiener filter by introducing frequency-dependent regularization. Since the backprojector is derived solely from the system PSF and regularization parameters, for the same optical system, it only needs to be precomputed once and can be directly called for the subsequent processing of all samples. The selection of parameters involves a trade-off between resolution enhancement and noise suppression. A detailed guide on parameter selection, as well as an analysis of the method's robustness against optical aberrations, is presented in S3–S5 of Supplement 1.

Figure 1(a) shows the spatial and Fourier domain representations of the forward projector f, illustrating the band-limited nature of the wide-field fluorescence OTF, particularly along the axial frequency dimension. Figure 1(b) compares the traditional matched backprojector and the proposed WB backprojector in both spatial and Fourier domains. While the matched backprojector yields a rapidly decaying spectral response, the WB backprojector produces a significantly flatter frequency response, leading to a more uniform spectral product with the forward projector. Figure 1(c) presents central cross-sections of the simulated 3D blurred object, which serves as the input for subsequent iterative deconvolution analysis.

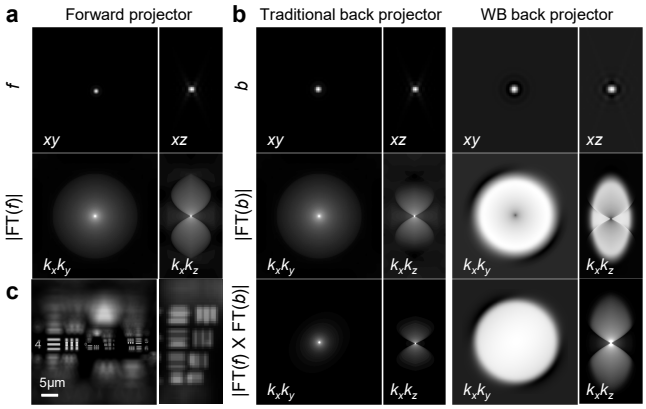

Fig. 1. Schematic of WB-ARL. (a) Central xy and xz cross-sections of the forward projector f in the spatial domain and Fourier domain. (b) Backprojector b for traditional RLD and WB-ARL in the spatial domain and Fourier domain. The third row shows the product of f and b in the Fourier domain. (c) Central xy cross-sections of the simulated 3D blurred object by the WF.

To quantitatively evaluate the performance of the proposed WB-ARL, we constructed a tilted USAF target as a 3D object as shown in Fig. 2(a). 3D reconstruction was performed using WB-ARL, compared with the traditional RLD. The simulation parameters were matched to the experimental setup in subsequent wide-field fluorescence experiments, specifically using a 40×/0.75 NA objective lens with a central wavelength of 550 nm. Spatial sampling parameters were configured as follows: xy-axis sampling interval is 162.5 nm, and z-axis sampling interval is 0.5 μm. As shown in Fig. 2(b), by using the WB backprojector, the product frequency response of the forward projector f and backprojector b becomes flatter, with faster iterative convergence speed. Figure 2(c) shows the comparison of image restoration results at different depths of the USAF target, including comparisons between traditional RLD and RLD with WB-ARL under both the same number of iterations and different numbers of iterations. Both traditional RLD and WB-ARL use the same forward projector operator f to equivalently affect the RLD process, but WB filtering uses an unmatched backprojector b that leads to faster convergence speed. When deconvolving blurred images, WB filtering produces the desired image reconstruction results more quickly, achieving results comparable to the traditional backprojector after 100 iterations with only 10 iterations.

To verify the performance of the proposed WB-ARL in improving processing speed and high-resolution reconstruction, we conducted experiments on wide-field fluorescence imaging experiments on *Pandorina morum* colonies, as shown in Visualization 1 and S6 of Supplement 1. We also applied WB-ARL to multichannel wide-field fluorescence imaging of mouse kidney tissue (Invitrogen FluoCells Prepared Slide #1), and the

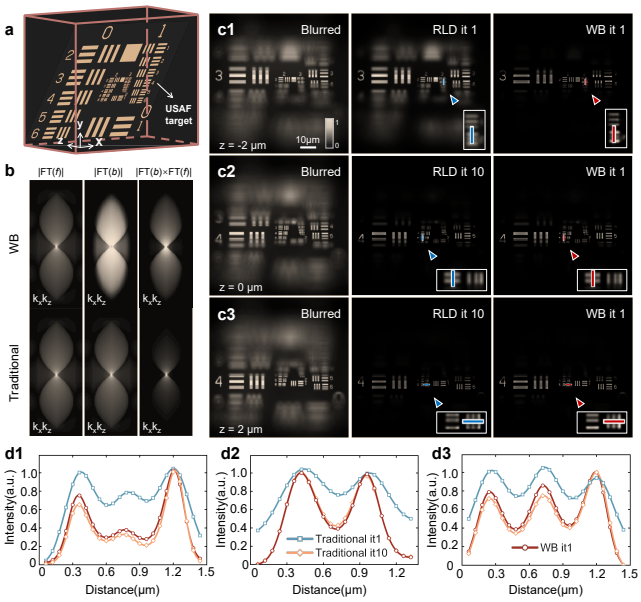

Fig. 2. WB-ARL simulation. (a) A 3D object composed of tilted USAF targets. (b) Central cross-sections in the k_x-k_z plane of the Fourier domain for the forward projector f and backprojector b, and their product. (c1)–(c3) Reconstructed results at different depths, comparing traditional RLD and WB-ARL. (d1)–(d3) Line profiles of the magnified regions in the matrices from (c1) to (c3).

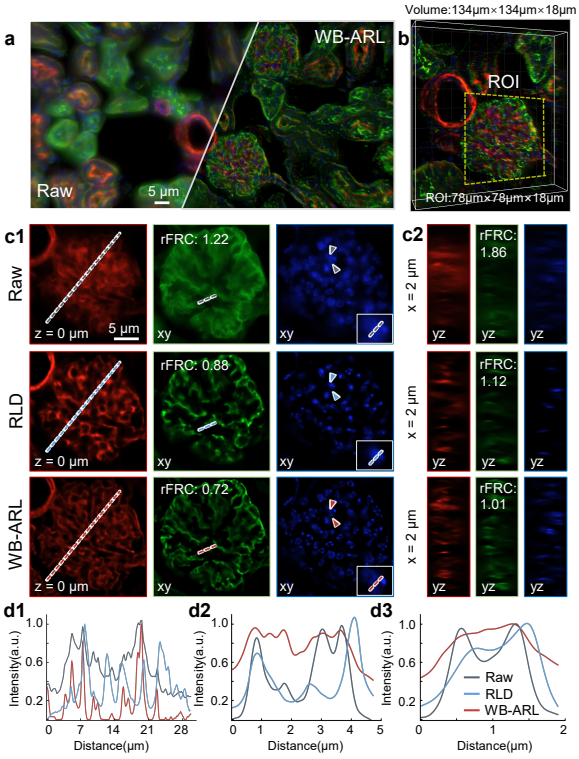

Fig. 3. Multichannel 3D wide-field fluorescence reconstruction of mouse kidney tissue. (a) Raw image of a mouse kidney section and WB reconstruction results after 5 iterations (green: glomeruli/tubules; red: F-actin; blue: nuclei). (b) 3D rendering of the glomerular region reconstructed by WB-ARL. (c1)–(c2) Magnified ROIs from (b), showing three-channel x–y and y–z raw images, RLD and WB-ARL reconstruction results. (d1)–(d3) Line profiles of the images in (c1). The results are shown in Visualization 2.

results are shown in Visualization 2. The experimental system was based on an objective lens (Zeiss Plan-Apochromat 20×/0.75 NA); the sampling interval of the z-axis was 0.2 μm, and the fluorescence emission central wavelengths were 600 nm, 519 nm, and 461 nm, respectively. Figure 3(a) comparatively shows the original wide-field image and the three-channel merged deconvolution result after only 5 iterations using the WB-ARL. Figure 3(b) displays a 3D rendering result of the glomerulus region we are interested in. For a more detailed comparison, Figs. 3(c) and 3(d), respectively show the original images and the WB-ARL reconstructed results of the three channels in the ROI of Fig. 3(b) at the central plane ($z = 0$), clearly demonstrating the pixel intensity changes along a specific line within the magnified area. We also use a rolling Fourier ring correlation (rFRC) method [19] to evaluate the images, where a smaller rFRC value indicates lower uncertainty and higher quality. It can be seen that the rFRC values under x–y sections are 1.22, 0.88, and 0.72, respectively, while those under x–z sections are 1.86, 1.12, and 1.01, respectively. It can be clearly seen that, compared to the blurred original image, WB-ARL, with a very small number of iterations, can reveal high-resolution structures within the glomerulus and improve image clarity and contrast.

We further validated the performance of WB-ARL on confocal fluorescence microscopy (Olympus FLUOVIEW FV3000) of a 3D cell phantom [20], as shown in Fig. 4. The experimental system employed a 100×/1.4 NA oil-immersion objective lens (Olympus UPLXAPO), with a z-axis sampling interval of 0.3 μm, lateral sampling interval of 0.0625 μm, and a fluorescence emission central wavelength of 520 nm. Figure 4(a) shows the tomographic view of the raw 3D cell phantom images, while Fig. 4(b) presents the cross-sectional view of the cell phantom. For a more detailed comparison, Figs. 4(c1) and 4(c2), respectively show the original images, RLD and the WB-ARL reconstructed results at x–y and x/y–z sections. Furthermore, rFRC analysis was performed to quantify the reconstruction quality. The WB-ARL method achieved the lowest rFRC value 0.66 compared to the original confocal image 0.96 and the traditional RLD result 0.67, and Figs. 4(d1)–4(d4) show the line profiles of the images in Figs. 4(c1) and 4(c2). It can be seen that the WB-ARL reconstructed images exhibit improvements in resolution and contrast compared to the blurred original images, with a better performance than traditional RLD. It can be verified that we significantly reduced the number of iterations required for deconvolution by utilizing WB-ARL, while ensuring reconstruction quality on both wide-field and confocal fluorescence microscopy systems.

Furthermore, we deeply parallelized the core computational steps of deconvolution reconstruction using CUDA (hardware platform: NVIDIA RTX 4060 GPU). Performance evaluation (as shown in Table 1) indicates that when processing typical data of 1024 × 1024 × 76 voxels, the C++ implementation corresponding to the traditional RLD method with 100 iterations takes as long as 1836 seconds. In contrast, our approach, combining WB-ARL (requiring only 10 iterations) and CUDA parallel optimization, achieves comparable imaging quality in just 4.6 seconds, resulting in an approximately 400-fold speedup compared with the CPU-based conventional RLD, with almost no loss in reconstruction accuracy. It is worth emphasizing that for larger datasets, the performance improvement of our

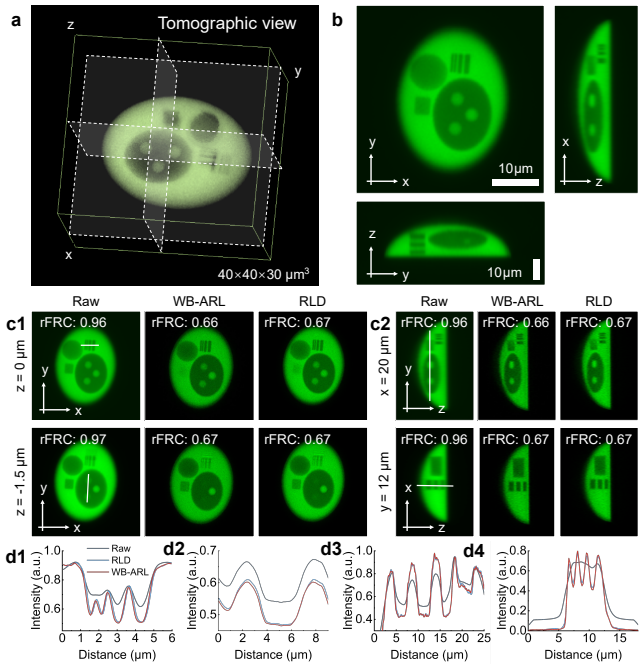

Fig. 4. Confocal 3D fluorescence reconstruction of cell phantom. (a) Tomographic view of the raw 3D cell phantom images; (b) cross-sectional view of the cell phantom; (c1)–(c2) x–y and x/y–z raw images, RLD and WB-ARL reconstruction results. (d1)–(d4) Line profiles of images in (c1) and (c2).

Table 1. Efficiency Comparison of WB-ARL across Different Platforms[a]

Task	Size	Matlab Time/Mem.	C++ Time/Mem.	Cuda Time/Mem.
WB backprojector calculation				
WB bp	$512^2 \times 76$	4 s/4.71 GB	6 s/3.47 GB	**1.7 s**/3.13 GB
WB bp	$781^2 \times 76$	7 s/5.24 GB	9 s/4.78 GB	**2.3 s**/4.71 GB
WB bp	$1024^2 \times 76$	12 s/6.62 GB	17 s/5.14 GB	**3.1 s**/4.89 GB
Deconvolution (Trad.: 100 iters/WB: 10 iters)				
Trad. bp	$512^2 \times 76$	105 s/4.9 GB	265 s/1.73 GB	11 s/2.95 GB
WB bp	$512^2 \times 76$	**14 s**/5.4 GB	35 s/1.86 GB	**1.3 s**/3.17 GB
Trad. bp	$781^2 \times 76$	345 s/6.8 GB	1035 s/2.92 GB	35 s/3.32 GB
WB bp	$781^2 \times 76$	**39 s**/7.3 GB	119 s/3.21 GB	**3.8 s**/3.47 GB
Trad. bp	$1024^2 \times 76$	540 s/8.7 GB	1836 s/6.5 GB	47 s/5.97 GB
WB bp	$1024^2 \times 76$	**65 s**/9.6 GB	217 s/6.9 GB	**4.6 s**/6.16 GB

[a]The bold values denote the shortest computation time, achieved by the WB-ARL method. All timings report end-to-end runtime for the specified task.

combined acceleration method will be even more significant, projected to reach a plateau of 400–500× before limited by the GPU memory capacity. We also compare WB-ARL with widely used Biggs–Andrews deconvolution methods [10] in S7 of Supplement 1.

In summary, we present WB-ARL, an accelerated RLD framework that employs an unmatched WB backprojector to flatten the spectral product with the system's OTF. By explicitly improving the eigenvalue clustering of the iterative operator, WB-ARL reduces the required iteration count by more than an order of magnitude while maintaining high reconstruction fidelity. When combined with CUDA-based parallelization, the proposed approach achieves an overall speedup of approximately 300–400× compared with CPU-based conventional implementations for large 3D fluorescence datasets containing tens of millions of voxels.

The WB-ARL framework provides insight into the convergence behavior of iterative deconvolution algorithms from a spectral perspective. Although the final reconstruction quality still depends on the accuracy of the system PSF, this limitation can be alleviated by incorporating advanced PSF estimation or aberration-correction strategies [21].

Funding. National Natural Science Foundation of China (NSFC), (62227818, 62361136588, 62305162, U21B2033, 62505136, 62575139); National Key Research and Development Program of China (2022YFA1205002, 2024YFF0505603, 2024YFF0505600, 2024YFE0101300); Biomedical Competition Foundation of Jiangsu Province (BE2022847) Key National Industrial Technology Cooperation Foundation of Jiangsu Province (BZ2022039); Fundamental Research Funds for the Central Universities (30923010206, 2023102001, 2024202002); National Key Laboratory of Plasma Physics (JCKYS2024212804); Open Research Fund of Jiangsu Key Laboratory of Spectral Imaging Intelligent Sense (JSGP202105, JSGP202201, JSGPCXZNGZ202401).

Disclosures. The authors declare no conflicts of interest.

Data availability. Data underlying the results presented in this paper are available in Ref. [22].

Supplemental document. See Supplement 1 for supporting content.

REFERENCES

1. C. Zuo, J. Li, J. Sun, *et al.*, Opt. Lasers Eng. **135**, 106187 (2020).
2. W. Yang and R. Yuste, Nat. Methods **14**, 349 (2017).
3. J. W. Lichtman and J.-A. Conchello, Nat. Methods **2**, 910 (2005).
4. W. H. Richardson, J. Opt. Soc. Am. **62**, 55 (1972).
5. L. B. Lucy, Astron. J. **79**, 745 (1974).
6. D. Sage, L. Donati, F. Soulez, *et al.*, Methods **115**, 28 (2017).
7. Y. Li, Y. Su, M. Guo, *et al.*, Nat. Methods **19**, 1427 (2022).
8. C. Su, Y. Gao, Y. Zhou, *et al.*, Bioinformatics **39**, btac760 (2023).
9. M. A. Bruce and M. J. Butte, Opt. Express **21**, 4766 (2013).
10. D. S. C. Biggs and M. Andrews, Appl. Opt. **36**, 1766 (1997).
11. H. Wang and P. C. Miller, IEEE Trans. Image Process **23**, 848 (2013).
12. R. Zanella, G. Zanghirati, R. Cavicchioli, *et al.*, Sci. Rep. **3**, 2523 (2013).
13. J. Mertz, *Introduction to Optical Microscopy* (Cambridge University Press, 2019).
14. G. L. Zeng and G. T. Gullberg, IEEE Trans. Med. Imaging **19**, 548 (2000).
15. S. Preibisch, F. Amat, E. Stamataki, *et al.*, Nat. Methods **11**, 645 (2014).
16. M. Guo, Y. Li, Y. Su, *et al.*, Nat. Biotechnol. **38**, 1337 (2020).
17. G. L. Zeng, Y. Weng, and G. T. Gullberg, IEEE Trans. Nucl. Sci. **44**, 98 (1997).
18. S. J. Glick and E. J. Soares, IEEE Trans. Nucl. Sci. **45**, 2183 (1998).
19. W. Zhao, X. Huang, J. Yang, *et al.*, Light Sci. Appl. **12**, 298 (2023).
20. M. Ziemczonok, A. Kuś, P. Wasylczyk, *et al.*, Sci. Rep. **9**, 18872 (2019).
21. R. Zhang, H. Du, N. Zhou, *et al.*, Laser Photonics Rev. **2025**, 2500032 (2025).
22. Z. Runnan "WB-ARL: Wiener–Butterworth accelerated Richardson–Lucy Deconvolution," Github (2025), https://github.com/RunnanZ/WB-ARL.